11

Mapping Aboveground and Foliage Biomass Over the Porcupine Caribou Habitat in Northern Yukon and Alaska Using Landsat and JERS-1/SAR Data

Wenjun Chen, Weirong Chen, Junhua Li, Yu Zhang, Robert Fraser, Ian Olthof, Sylvain G. Leblanc and Zhaohua Chen
Canada Centre for Remote Sensing, Natural Resources Canada
Canada

1. Introduction

The linkage between caribou and the aboriginal people in the North America has existed for thousands of years. Caribou have played a critical role in the economy, culture, and way of life of the aboriginal people (Hall, 1989; Madsen, 2001). Currently, there are 60 major migratary tundra caribou herds circum-arctic, of which 30 are located in North America, including the Porcupine caribou herd in northern Yukon, Canada and northern Alaska, USA (Russell et al., 1992; Russell et al., 1993; Russell & McNeil, 2002; Russell et al., 2002; Griffith et al., 2002). The Porcupine caribou herd has been at the centre of debate between wildlife habitat conservation and industrial development in the Arctic because of the potential oil drilling in the Arctic National Wildlife Refuge (ANWR) 1002 area, which happens to largely overlap with the calving ground of the Porcupine caribou herd (Griffith et al., 2002; Kaiser, 2002; National Research Council, 2003; Heuer, 2006).

One of the objectives of the Canadian International Polar Year (IPY) project entitled "Climate Change Impacts on Canadian Arctic Tundra Ecosystems (CiCAT): Interdisciplinary and Multi-scale Assessments" was to assess the impact of climate change on caribou habitats over Canada's north, in close collaboration with the CircumArctic Ranfiger Monitoring and Assessment network (CARMA) (http://www.rangifer.net /carma/). Because of the vastness and remoteness of the arctic landmass, inherent logistic difficulty, and high cost of conducting field measurements, an approach that is solely based on field inventory is clearly impractical for monitoring and assessing the impact of climate on caribou habitats. Satellite remote sensing can monitor land surfaces from space repeatedly and consistently over large areas. Therefore, remote sensing provides a powerful tool for monitoring and assessing the impact of climate on caribou habitats, when calibrated and validated against the field measurements and other independent data.

In this study, we report the development of baseline maps of aboveground and foliage biomass over the Porcupine caribou habitat in northern Yukon and Alaska, using Landsat and JERS-1/SAR data. Specifically, we will (1) describe aboveground and foliage biomass measurement, (2) establish and validate relationships between measurements and remote sensing indices, and (3) map aboveground and foliage biomass for the Porcupine caribou habitat.

2. Data sources and methods

2.1 Field measurements of aboveground and foliage biomass

Field measurements were made in Yukon and North Western Territories (Fig. 1). Aboveground biomass was measured at 43 sites in the summer of 2004 along the Dempster Highway, which goes through the winter and summer ranges of the Porcupine caribou habitat (Fig. 1). Foliage biomass was measured at 10 non-treed sites along the Dempster Highway in the summer of 2006, and again in the summer of 2008 at 11 non-treed sites in the Ivvavik National Park. The Ivvavik National Park is located at northern tip of the Yukon and overlaps with the calving ground and summer range of the Porcupine caribou herd. Details of measurement procedure, calculation method, and results are described as follows.

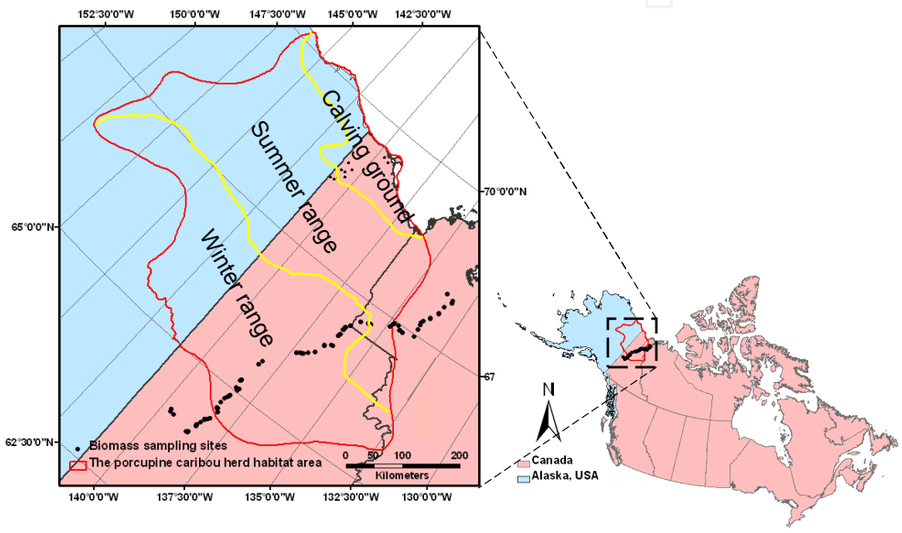

Fig. 1. Locations of the Porcupine caribou calving ground, summer range, and winter range, as well as that of the aboveground and foliage biomass measurement sites along the Dempster Highway transect during the summers of 2004 and 2006, and in the Ivvavik National Park during the summer of 2008.

We selected sites that were representative of local vegetation conditions, relatively homogenous, and of size at least 3 × 3 Landsat pixels (i.e., > 90 m × 90 m), to ensure that the field measurements can be reliably correlated with Landsat-scale remote sensing indices. In the north where the growing season is very short, biophysical parameters (e.g., foliage biomass) vary significantly both during the beginning and end of the growing season, but are relatively stable and achieve their maximums during the middle of the growing season. Therefore, we measured aboveground biomass and foliage biomass during middle of growing season (e.g., July 18-27, 2004, July 19-27, 2006, and July 15-26, 2008).

We used a systematic approach to sample and measure the aboveground biomass: layer by layer from top to the ground. If a site was sparsely treed woodland, we first measured tree biomass with a variable sampling plot scheme using a prism (Halliwell & Apps, 1997). The basic principle of the variable sampling plot scheme is that each tree is selected using a circular plot with a radius r that is proportional to its diameter at the breast height (DBH). The constant of proportionality is called the plot radius factor (PRF), and thus for tree i we can write:

$$PRF = r_i / DBH_i \quad or \quad r_i = PRF \times DBH_i \tag{1}$$

with *DBH* is in centimeters and plot radius is in meters, *PRF* is in m cm^{-1}. A tree is included or "in" if $DBH_i > r_i/PRF$, and excluded or "out" otherwise. A difficulty may arise as whether to include or exclude a tree if it's at the edge, namely, $DBH_i \approx r_i/PRF$. If this is the case, the distance from the plot centre to the tree is measured. Using the tree's *DBH* and the appropriate PRF, this distance can then be compared to the radius of the plot as calculated by equation 1, and the tree place "in" or "out" of the plot after-the-fact. The measurements included tree height, diameter at breast height (*DBH*), and stand density. The heights of trees are recorded using a laser height measurement instrument (Impulse Forest Pro, Lasertech, Clarkston, MI, USA). Trees for height measurement are selected on basis of the point plot scheme. The value of *DBH* was measured using a tape. The stocking and biomass of the trees were then calculated on basis of allometric equations.

If tree regeneration was present, we measured the biomass of the seedlings using a fixed circular plot of radius of 3.99 m. The measurements included counting the number of stems per tree species, selecting an average-sized seedling to estimate its ground stem diameter, height, and sampling one or two average-sized seedling to measure its fresh and oven-dry weight.

For the understory layers, namely, high shrub, low shrub, herbs/graminoids, moss, and lichen, we harvested samples at five 1 m × 1 m plots to measure the total aboveground biomass: four at four directions and one random (Fig. 2). All the aboveground biomass within the plots were cut and collected into plastic bags and their green biomass weighed. Out of the five plots, we selected one representative plot to conduct an intensive sampling. For this plot, we measured the average height, visually estimate the ground cover percentage, and then cut and weighed the fresh biomass, sequentially, for tall shrub, low shrubs, herbs/graminoids, moss, and lichen. The ratio of green to oven-dry biomass was measured by bringing a sample of the aboveground biomass from the plot back to laboratory.

If a site had no trees, then we applied the aforementioned understory procedure. Note that the plot number and design of a specific site were determined on basis of site conditions: the more heterogeneous and sparse the vegetation is at a site, the more plots are needed (Chen et al., 2009b; Chen et al., 2010b). The procedure was modified for tall shrubs if the tall shrubs (higher than 50 cm) were clustered instead of homogeneous distribution. Our field experience indicated that it was often the case for tall shrubs. In this case, we measured the biomass of tall shrubs using a fixed circular plot of radius = 3.99 m. The measurements included identifying shrub species, counting number of clusters of shrub in the plot, and selecting two average-sized clusters of shrub for more extensive sampling. All aboveground biomass of the two clusters of shrub were cut and weighed for total green biomass. A fraction of the biomass was brought back to measure the ratio of oven-dry to fresh weight. If there are more than one tall shrub species, we repeated the measurements for each of them. The procedure for low shrub, herbs/graminoids, moss, and lichen remain the same.

For foliage biomass measurement during the summers of 2006 and 2008, we selected only non-treed sites. At each sites, five 1 m × 1 m plots were sampled (Fig. 3). Fig. 3 shows a photograph of the field sampling at a coastal plain site in the Ivvavik National Park during the summer of 2008. At each plot, all plants were harvested, sorted into dead and live, different species, and leaves and stem, and recorded for their fresh weights. A fraction of the harvested biomass for all components were brought back to the laboratory, oven-dried, and

weighed. Oven-dry foliage biomass of vascular plants were than calculated using the ratio of oven-dry to fresh foliage biomass and the corresponding fresh weight records.

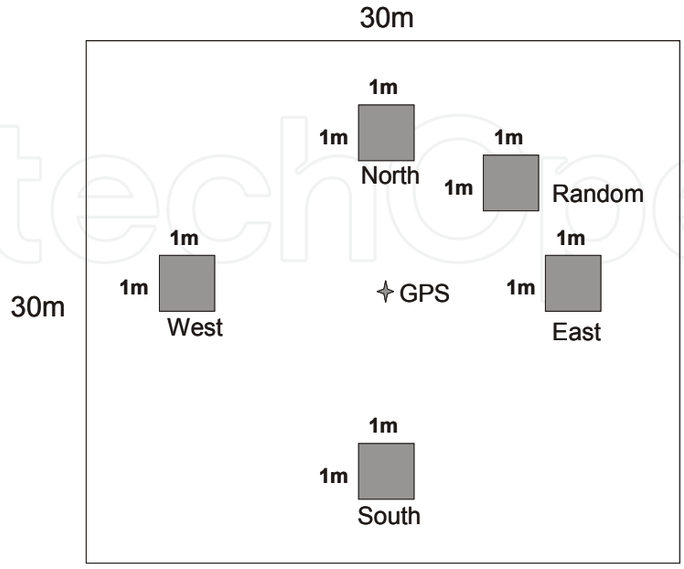

Fig. 2. Plot design for measuring aboveground and foliage biomass at non-forested sites.

The tree oven-dry aboveground biomass at a woodland site was calculated using Canada-wide tree biomass equations by Evert (1985) and the Weibull tree-size distribution function within a stand by Chen (2004).

In order to determine the tree-size distribution for a woodland site, the Parameter Prediction Method (PPM) based on basal area was implemented (Chen, 2004). With measured average *DBH*, height, and stand density (trees ha^{-1}) as inputs, the tree-size distribution function gives 15 tree-size classes for each site, and output mean DBH, height, and number of trees for each class. Here, we used trembling aspen functions for hardwood species, jack pine functions for all pine species and pine-mixture, black spruce functions for all spruce and fir species, and mixed-stand function for mixed softwoods/hardwoods.

The Canada-wide biomass equations calculate the oven-dry biomass of stem, bark, and crown of a single tree for 18 Canadian tree species (Evert, 1985), with a given DBH and height. Using the information of tree-size distribution and the biomass equations, we first calculated each biomass component (stem, bark, and crown), added these components to get total aboveground biomass, and then multiplied with the number of trees in each tree-size distribution class to get the total tree biomass per hectare, B_t, in t ha^{-1}.

The aboveground oven-dry biomass of clustered high shrub and regenerating trees at a site, B_s in t ha^{-1}, was calculated by

$$B_s = \frac{(b_{s1} + b_{s2})}{2} \frac{N_c}{5} R_s \tag{2}$$

where $(b_{s1} + b_{s2})/2$ is the mean green biomass of the two clusters of shrub sampled or that of regenerating trees (kg per cluster or regenerating tree), N_c is the number of clusters of shrub or regenerating trees in the 3.99 m-radius plot, and R_s is the ratio of oven-dry to fresh biomass for shrub or the regenerating trees.

Fig. 3. Photograph showing biomass sampling at a coastal plain site in the Ivvavik National Park, July 25, 2008. Front are 3 northern students from Aklavik, NWT (left to right: Alexander Gordon, Jayneta Pascal & Kayla Arey), and at the background Weiroing Chen of CCRS was sampling root biomass (photo by Wenjun Chen).

The aboveground oven-dry biomass of graminoids, herbs and shrubs in the lower layers, B_g in t ha^{-1}, was calculated by

$$B_g = \frac{(b_{g1} + b_{g2} + b_{g3} + b_{g4} + b_{g5})}{5} 10 R_g \tag{3}$$

where b_{g1}, b_{g2}, b_{g3}, b_{g4}, and b_{g5} are, respectively, the aboveground green biomass of the graminoids/herbs and shrubs mixture for each of the five plots in a site (kg m^{-2}), and R_g is the ratio of oven-dry to fresh biomass for the mixture of graminoids/herbs and shrubs. The oven-dry biomass of lichen, B_l in t ha^{-1}, was calculated by

$$B_l = \frac{(p_{l1} + p_{l2} + p_{l3} + p_{l4} + p_{l5})}{5} \frac{(b_{l1} + b_{l2})}{2} 1000 R_l \tag{4}$$

where P_{l1}, P_{l2}, P_{l3}, P_{l4}, and P_{l5} are, respectively, the percentage of lich ground cover at the 5 plots, b_{l1} and b_{l2} are, respectively, the fresh lichen biomass of each of the two 10-cm by 10-cm samples collected from one of the plots (kg m^{-2}), and R_l is the ratio of oven-dry to fresh biomass for lichen. The oven-dry biomass of live moss, B_m in t ha^{-1}, was calculated by

$$B_m = \frac{(p_{m1} + p_{m2} + p_{m3} + p_{m4} + p_{m5})}{5} \frac{(b_{m1} + b_{m2})}{2} 1000 R_m D_m \tag{5}$$

where P_{m1}, P_{m2}, P_{m3}, P_{m4}, and P_{m5} are, respectively, the percentage of moss ground cover at the 5 plots, b_{m1} and b_{m2} are, respectively, the aboveground green biomass of each of the two 1-cm depth, 10 cm by 10 cm square moss samples collected from one of the plots (kg m^{-2}), D_m is the depth of alive moss in cm, and R_m is the ratio of oven-dry to green biomass for moss. The aboveground biomass for a site, B_a, was thus the summation of all these components where proper.

The calculation of foliage biomass, B_f in unit g m^{-2}, was similar to that of aboveground biomass, except that only the foliage component of vascular plants was included.

2.2 Remote sensing data sources and processing

Nearly clear-sky Landsat TM/ETM+ level 1G orthoimagery was downloaded from the United Stated Geological Survey (USGS) website (http://earthexplorer.usgs.gov) and from the Centre for Topographic Information (CTI) of Natural Resources Canada, available through Geogratis (http://geogratis.cgdi.gc.ca/). 23 scenes are needed to cover the entire Porcupine caribou habitat. Most of them were acquired within the middle growing season (July 10 to August 15) during 1999 – 2003. Only Bands 3 (0.63–0.69 μm), 4 (0.75–0.90 μm), and 5 (1.55–1.75 μm) were used in the study, because Bands 1-3 are highly correlated, as are Bands 5 and 7. Prior to further analysis, all scenes, if necessary, were re-projected to Lambert Conformal Conic (LCC) projection with 95° W, 49° N as the true origin and 49° N and 77° N as standard parallels. Surface reflectance was derived by radiometrically normalizing each scene to 250 m resolution clear sky MODIS imagery, which was a 10-day composite acquired during July 21-31, 2001 with matching bands calibrated to a strip of atmospherically corrected Landsat TM/ETM+ images. A Landsat mosaic of surface reflectance was then generated with further normalizations for individual scenes if substantial discrepancy exists. All radiometric normalization and calibration equations were developed using a Scattergram Controlled Regression method (Elvidge et al., 1995; Yuan & Elvidge, 1996; Chen et al., 2010a). Furthermore, clouds and forested areas were removed and masked, and the mosaic was clipped based on the Porcupine caribou habitat boundary.

The JERS-1/SAR datasets were extracted from the North America JERS mosaics (acquired in the summer of 1998) to cover the Porcupine caribou habitat (Kyle McDonald, JPL, personal communication). In addition, data of 1:50000 DEM covering the habitat were also obtained for orthorectifying the JERS mosaic. The North America JERS summer mosaics were not precisely geo-referenced, because topographic distortions were not removed during the mosaic process due to the lack of adequate DEM (Sheng & Alsdorf, 2005). Visual inspection showed that the offset between the JERS mosaic and the Landsat images may be 300 m ~ 5000 m. The positioning error was expected to be much larger in mountainous regions.

In this study, we employed a SAR image simulation method from DEM data to correct topographic distortions (Sheng & Alsdof, 2005). Briefly speaking, this method includes four steps: (1) simulating a SAR image in an azimuth-range projection from the DEM according to imaging geometry of real SAR image; (2) collecting ground control points that tie the uncorrected SAR image to the simulated SAR image; (3) warping the real SAR image to the simulated SAR image using a polynomial function fitted from the ground control points; and (4) projecting the warped real SAR image back to the DEM map coordinate system. The method requires three types of inputs: individual scene of SAR imagery, DEM data, and SAR imaging geometry parameters (i.e. sensor altitude H, minimum look angle θ, the orbital azimuth angle β). Since the year-day file, which contains the date of specific JERS image's acquisition, was delivered with the JERS mosaics data, we could extract individual path image in the JERS mosaic. The path image was used as an input in place of individual scene of JERS. In addition, since the imaging geometry information of the individual path in the JERS mosaic was unavailable, general JERS imaging geometry parameters were used in the SAR simulation method. For the purpose of image matching for ground control point selection, a correct geometry was preferred but is not necessary (Sheng and Alsdof, 2005;

Linder and Meuser; 1993). In this study, we used H = 568000 meter, θ =35 degree, and β =190 degree in SAR image simulation. Finally, the Digital Number (DN) values of JERS mosaic could be converted to backscatter coefficients σ (in db format) by the equation:

$$\sigma = 20 \times \log_{10} DN - 48.54 \tag{6}$$

The co-registered and geo-referenced Landsat TM/ETM+ and JERS-1 mosaics were then compared with measurements of aboveground and foliage biomass, with their best-fit relationships being applied back to the mosaics to produce maps of aboveground and foliage biomass over the Porcupine caribou habitat, as outlined in Fig. 4.

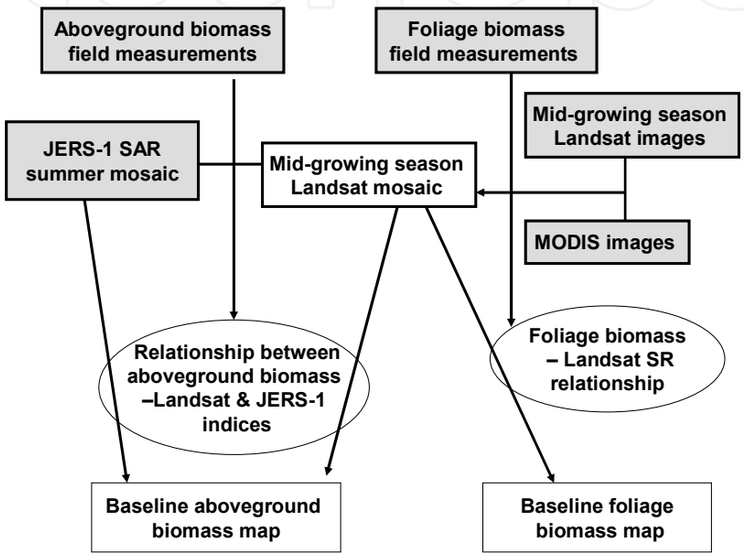

Fig. 4. Flow chart describing the procedures of using field measurements and remote sensing data to produce aboveground and foliage biomass baseline maps.

3. Results and discussions

3.1 Measured aboveground and foliage biomass over the Porcupine caribou habitat

Table 1 summarizes the mean value, standard deviation, and range of aboveground biomass measured at sites within and around the Porcupine caribou winter and summer range along the Dempster Highway, Yukon, during the summer of 2004. Average values of measured aboveground biomass of sparsely treed woodland, low-high shrub lands, and mixed graminoids-dwarf shrub-herb lands were, respectively, 57.3, 11.1, and 2.3 t ha^{-1}. Within each vegetation type, the ranges of measured aboveground biomass were very large. The standard deviations of measured aboveground biomass among sites were often larger than their corresponding mean values, especially for low-high shrubs and mixed graminoids-dwarf shrub-herb, and when all types of vegetation were considered. The measured aboveground biomass ranged from 10 to 100 t ha^{-1} for sparsely treed woodlands, from 1 to 100 t ha^{-1} for the low-high shrub sites, from 0.5 to 10 t ha^{-1} for mixed graminoids-dwarf shrub-herb sites. These measurements indicate that there are significant overlaps in the ranges of aboveground biomass between sparsely treed woodlands and low-high shrub sites, and between low-high shrub sites and mixed graminoids-dwarf shrub-herb sites.

Dominant vegetation type	Mean (t ha^{-1})	Standard deviation (t ha^{-1})	Range (t ha^{-1})	Number of sites
Sparse woodland	57.3	34.0	9.1 – 94.5	8
Low-high shrub	11.1	11.4	2.0 – 47.2	19
Graminoids-dwarf shrub	2.3	2.2	0.4 – 8.3	16
All types	16.4	25.6	0.4 – 94.5	43

Table 1. Mean value, standard deviation, and range of aboveground biomass measured at sites within and around the Porcupine caribou winter and summer range along the Dempster Highway, Yukon, during the summer of 2004.

	Dominant vegetation type	Mean	Standard deviation	Range	Number of sites
Foliage biomass (g m^{-2})	Low-high shrub	135.4	36.3	95.3 – 198.4	6
	Graminoids-dwarf shrub	65.3	16.3	37.9 – 92.3	9
	Coastal tussock	87.9	22.2	63.1 – 106.1	3
	Rock lichen	11.3	10.2	0.0 – 20.0	3
	All types	80.8	47.2	0.0 – 198.4	21
Abovegro und biomass (t h^{-1})	Low-high shrub	7.02	7.58	0.36 – 18.16	6
	Graminoids-dwarf shrub	3.11	2.64	0.32 – 8.55	9
	Coastal tussock	0.77	0.53	0.21 – 1.27	3
	Rock lichen	0.65	0.57	0.0 – 1.06	3
	All types	3.54	4.83	0.0 – 18.16	21

Table 2. Mean value, standard deviation, and range of foliage biomass measured at sites within and around the Porcupine caribou winter and summer ranges along the Dempster Highway, Yukon during the summer of 2006, as well as at sites within and around the Porcupine caribou calving ground and summer range inside the Ivvavik National Park, Yukon during the summer of 2008. Also shown are statistics for the corresponding aboveground biomass measurements.

Similarly, the foliage biomass values measured at sites within a specific dominant vegetation type also varied significantly (Table 2). For example, foliage biomass ranges from 95.3 to 198.4 g m^{-2} for low-high shrub sites, 37.9–92.3 g m^{-2} for mixed graminoids-dwarf shrub-herb sites, 63.1–106.1 g m^{-2} for coastal plain tussock sites, and 0.0–20.0 g m^{-2} for hill-top rock lichen sites. Consequently, assigning aboveground or foliage biomass value to a site according to its vegetation type can result in substantial error (Gould et al., 2003; Walker et al., 2003).

3.2 Relationships between aboveground biomass and remote sensing indices

In this study, we investigated the applicability of both optical and radar data as well as their combinations. To obtain the best regression model for estimating aboveground biomass, robust multiple regressions were conducted between field-measured aboveground biomass and various remote sensing-derived variables such as TM spectral reflectance, vegetation

indices, and JESR-1/SAR backscatter coefficients. We used 3 × 3 pixels (i.e., 90 m by 90 m) averaged value in place of single pixel value in order to reduce the effect of erroneous spectral features, e.g., features of adjacent pixels may have been assigned to some field plots of the data due to errors in image registration and the location of sample plots. The Landsat images were re-sampled to 100 m resolution for matching the resolution of the North America JERS summer mosaic.

For the sites along the Dempster Highway, we found that strong correlations exist between $\ln(B_a)$ and remote sensing signals (Table 3). When all types were mixed, the strongest correlation was found against the L-band JERS-1/SAR backscatter, followed by the Landat B4/B5 (Fig. 5). The Landsat bands 3 and 5 show strong negative relationships for the sparse woodlands and all types mixed, but not for shrub and graminoids lands.

		B3	B4	B5	B4/B5	SR	NDVI	SWVI	JERS
Sparse woodland	r	**-0.77**	**-0.18**	**-0.78**	**0.40**	**0.53**	**0.21**	**0.44**	**0.68**
	r^2	0.59	0.03	0.61	0.16	0.28	0.04	0.19	0.46
Low-high-Shrub	r	**-0.17**	**0.04**	**-0.39**	**0.59**	**0.47**	**0.26**	**0.59**	**0.42**
	r^2	0.03	0.00	0.15	0.35	0.22	0.07	0.35	0.18
Graminoids-dwarf shrub	r	**-0.13**	**0.22**	**0.01**	**0.21**	**0.26**	**0.31**	**0.18**	**0.64**
	r^2	0.02	0.05	0.00	0.04	0.07	0.10	0.03	0.41
All types	r	**-0.65**	**-0.02**	**-0.68**	**0.70**	**0.63**	**0.53**	**0.68**	**0.73**
	r^2	0.42	0.00	0.46	0.49	0.40	0.28	0.46	0.53

Table 3. Correlation coefficient (r) and coefficient of determination (r^2) between $\ln(B_a)$ and remote sensing indices for mixed graminoids-dwarf shrub-herb, low-high shrub, sparse woodlands, and all types for aboveground biomass measurements along the Dempster Highway in 2004. Remote sensing indices include Landsat red band reflectance (B3), near infrared band reflectance (B4), shortwave infrared band reflectance (B5), ratio of B4/B5, simple ratio (SR = B4/B3), normalized differential vegetation index (NDVI = (B4 - B3)/(B4 + B3)), shortwave vegetation index (SWVI = (B4 - B5)/(B4 + B5)), and L-band JERS-1/SAR backscatter coefficient (JERS).

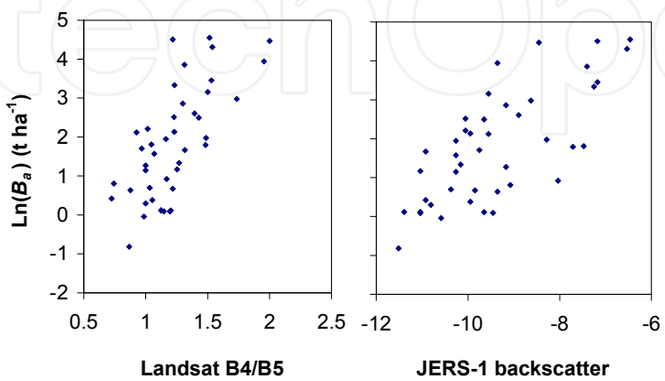

Fig. 5. Scatter plots between $\ln(B_a)$ and Landsat B4/B5 as well as JERS-1/SAR backscatter coefficients.

Many vegetation indices have been developed and applied for estimating aboveground biomass (Anderson & Hanson, 1992; Anderson et al., 1993; Mutanga & Skidmore, 2004; Lu 2005). In Table 3, we examined 4 vegetation indices: ratio of Landsat B4/B5, simple ratio (SR = B4/B3), normalized differential vegetation index (NDVI = (B4 - B3)/(B4 + B3)), shortwave vegetation index (SWVI = (B4 - B5)/(B4 + B5)). In general, vegetation indices can partially reduce the impacts on reflectance caused by environmental conditions and shadows, thus improve correlation between AGB and vegetation indices, especially in those sites with complex vegetation stand structures (Lu et al., 2004). However as shown in Table 3, not all vegetation indices are significantly correlated with aboveground biomass. Consequently, various degrees of success had been obtained in estimating aboveground biomass using Landsat vegetation indices (Sader et al., 1989; Lee & Nakane, 1996; Nelson et al., 2000; Steininger, 2000; Foody et al., 2003; Phua & Saito, 2003; Zheng et al., 2004). For example, Nelson et al. (2000) found that aboveground biomass cannot be reliably estimated using Landsat data without the inclusion of secondary forest age. Steininger (2000) explored the ability of Landsat data for estimating aboveground biomass of tropical secondary forests and found that saturation was a problem for advanced successional forests.

Similarly, different degrees of success had been obtained in previous studies of using radar data for estimating aboveground biomass, with longer-wavelength L-band and P-band SAR data proven to be more valuable (Sader, 1987; Le Toan et al., 1992; Rauste et al., 1994; Ranson et al., 1997; Luckman et al., 1997; Kurvonen et al., 1999; Kuplich et al., 2000; Tsolmon et al., 2002; Sun et al., 2002; Castel et al., 2002; Santos et al., 2002). For example, Kuplich et al. (2000) used JERS-1/SAR data for aboveground biomass estimation of regenerating forests. Sun et al. (2002) found that multi-polarization L-band SAR data were useful for estimating aboveground biomass of forest stands in mountainous areas. Castel et al. (2002) identified the significant relationships between the backscatter coefficient of JERS-1/SAR data and the stand biomass of a pine plantation. Santos et al. (2002) used JERS-1/SAR data to analyse the relationships between backscatter signals and biomass of forest and savanna formations. The significant correlation between aboveground biomass and JERS-1/SAR backscatter coefficient, as shown in Table 3 and Fig. 4, indicates that longer-wavelength L-band SAR data are also valuable in the Arctic. Nevertheless, the saturation problem is also common in estimating aboveground biomass using radar data (Luckman et al., 1997; Balzter, 2001, Lucas et al., 2004; Kasischke et al., 2004). For example, Luckman et al. (1997) found that the longer-wavelength L-band SAR image was more suitable to discriminate different levels of forest biomass up to a certain threshold than shorter-wavelength C-band SAR data.

To take advantages of the ability of Landsat vegetation indices and JERS-1/SAR backscatter coefficient, we used both data for estimating aboveground biomass. The best fit relationship between aboveground biomass and JERS-1/SAR backscatter coefficient σ as well as Landsat B4/B5 for all types mixed in the Dempster Highway study area is given by:

$$\ln(B_a) = 2.3759(\mathrm{B4/B5}) + 0.5542\sigma + 4.0948\,, \tag{7}$$

with a coefficient of determination r^2 = 0.72, and standard estimation error (*SEE*) = 0.78. Because the logarithmic equations could introduce a systematic bias when used for back calculating biomass, it has now become fairly widely recognized that a correction factor is necessary to counteract this bias (Sprugel, 1983). The correction factor (*CF*) can be calculated by using the formula:

$$CF = e^{SEE^2/2} \tag{8}$$

For equation (7), the *CF* = 1.35. The 1:1 comparison of estimated aboveground biomass using *CF*-corrected equation (7) and the measured values for the sites along the Dempster Highway is shown in Fig. 6, with the slope = 0.95, r^2 = 0.72, and *SEE* = 13.5 t h^{-1} over measured aboveground biomass range from 0.4 to 94.5 t h^{-1}. These results agreed well with the finding of Moghaddam et al. (2002) that the estimation accuracy of forest biomass was significantly improved when radar and optical data were used in combination, compared to estimates using a single data type alone.

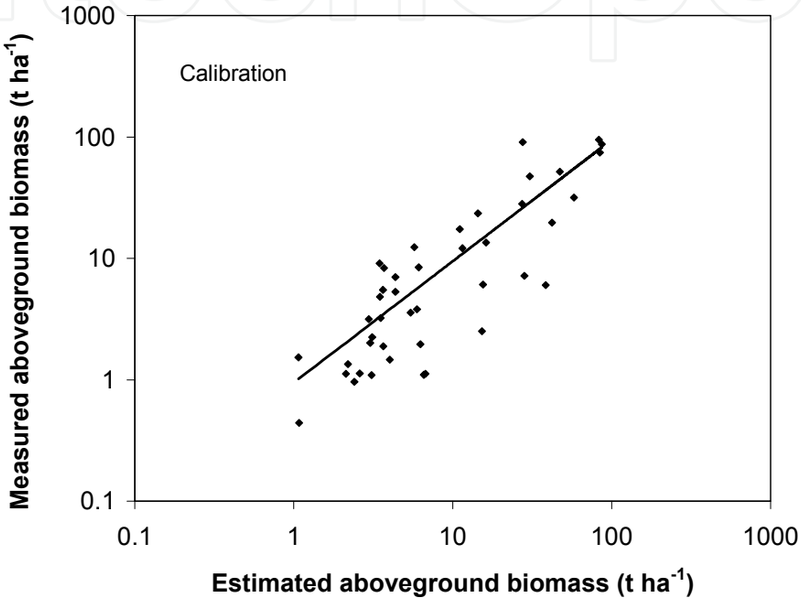

Fig. 6. A 1:1 comparison between estimated and measured aboveground biomass values for the calibration sites along the Dempster Highway transect measured during the summer of 2004. For clarity over the low biomass range, the results are shown on the log-log scale.

3.3 Validation of aboveground biomass relationship with remote sensing indices

In a previous study (Chen et al., 2009a), we validated equation (7) using aboveground biomass measurements at 33 sites around Yellowknife, Northwest Territories, and Lupin Gold Mine, Nunavut Territories. The 1:1 comparison of estimated aboveground biomass and the measurements for the Yellowknife and Lupin Gold Mine study area indicates that the equation holds up very well, with r^2 = 0.81, slope =1.17, and *SEE* = 9.67 t h^{-1} over measured aboveground biomass range from 0.9 to 103.3 t h^{-1}.

In this study, we further validated the relationship using measurements collected over the same study area at later dates. We used aboveground biomass measured at 21 sites along the Dempster Highway during the summer of 2006 in the Ivvavik National Park during the summer of 2008, where foliage biomass was the main measurement target, to validate the above relationship. Fig. 7 shows the validation result, with the slope = 0.91, r^2 = 0.90, and *SEE* = 1.5 t h^{-1} over measured aboveground biomass range from 0 to 18.16 t h^{-1}.

These validation results suggest that the aboveground biomass can be reliably estimated using Landsat B4/B5 and JERS-1/SAR backscatter coefficient.

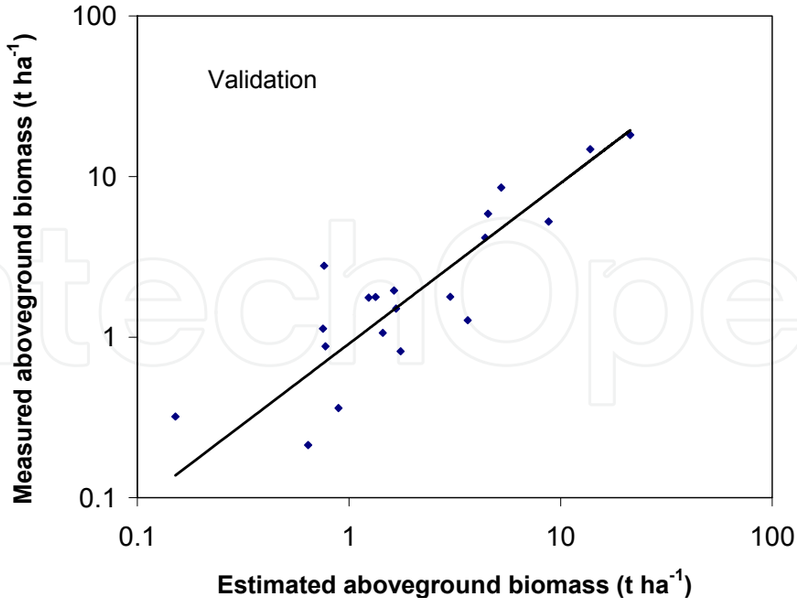

Fig. 7. A 1:1 comparison between estimated and measured aboveground biomass values for the validation sites along the Dempster Highway transect measured during the summer of 2006 and in the Ivvavik National Park during the summer of 2008. For clarity over the low biomass range, the results are shown on the log-log scale.

3.4. Relationships between foliage biomass and remote sensing indices

As shown in Table 4, the Landsat-based *SR* can explain 81% variations in measured foliage biomass within the Porcupine caribou habitat. The explanation power of other Landsat-based indices in the descending order is 76% for the ratio of B4/B5, 71% for SWVI, and 67% for NDVI. Single band reflectance of Landsat has lower power of explanation.

	B3	B4	B5	SR	NDVI	B4/B5	SWVI
r	**-0.73**	**0.52**	**-0.54**	**0.90**	**0.82**	**0.87**	**-0.84**
r^2	0.53	0.27	0.29	0.81	0.67	0.76	0.71
SEE	**31.4**	**39.1**	**38.6**	**20.6**	**26.4**	**21.9**	**25.2**

Table 4. Correlation coefficients (*r*), coefficient of determination (r^2), and standard estimation error (*SEE*, in g m^{-2}) between foliage biomass (B_f) and remote sensing signals for foliage biomass measured at the 21 sites along the Dempster Highway in 2006 and in the Ivvavik National Park in 2008. Remote sensing indices include Landsat red band reflectance (B3), near-infrared band reflectance (B4), shortwave infrared band reflectance (B5), ratio of B4/B5, simple ratio (SR = B4/B3), normalized differential vegetation index (NDVI = (B4 - B3)/(B4 + B3)), and shortwave vegetation index (SWVI = (B4 - B5)/(B4 + B5)).

In comparison with results for aboveground biomass shown in Table 3, Landsat-based vegetation indices have a much improved power of explanation for foliage biomass (Table 4). This is in good agreement with the fact that optical sensors mainly capture canopy information, thus the optical sensor data are more suitable for estimation of canopy parameters such as foliage biomass than aboveground biomass, as demon stared by

previous studies (Franklin & Hiernaux, 1991; Hall et al., 1995; Chen & Cihlar 1996; Turner et al., 1999; Brown et al., 2000; Chen et al., 2002; Wylie et al., 2002; Phua & Saito, 2003; Laidler & Treitz, 2003; Lu, 2004). The best fit relationship between foliage biomass (B_f, g m^{-2}) and Landsat-based simple ratio (SR) over the Porcupine caribou habitat is given as follows

$$B_f = 16.62SR - 1.1906 , \quad (9)$$

with r^2 = 0.81, SEE = 20.6 g m^{-2}, F= 81, P = 2.7×10^{-8}, and n = 21 (Fig. 8).

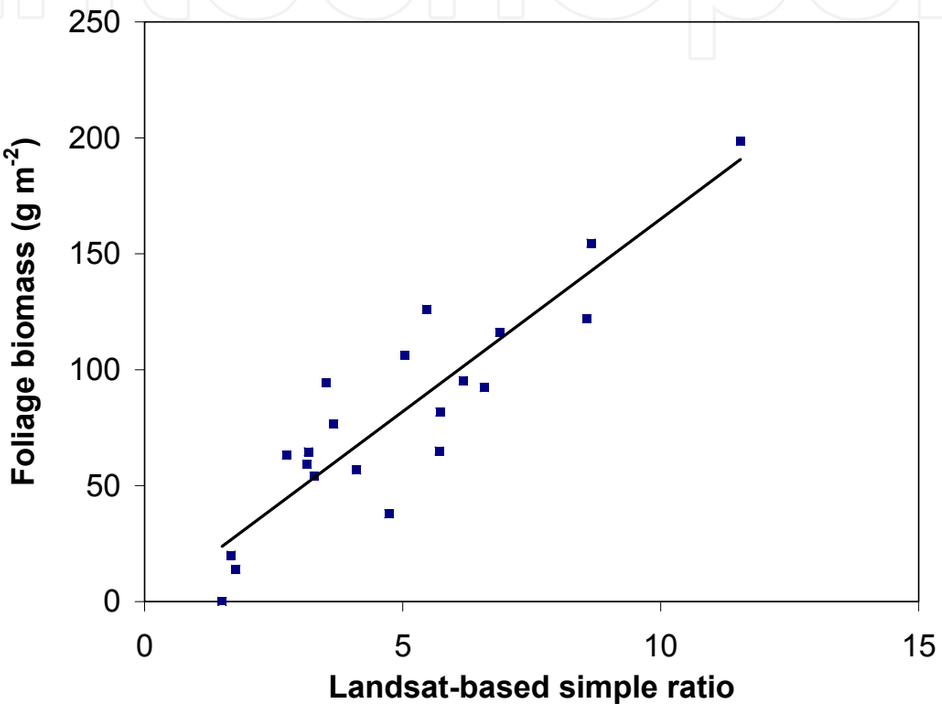

Fig. 8. Relationship between Landsat simple ratio and foliage biomass measured at sites along the Dempster Highway during the summer of 2006 and in the Ivvavik National Park during the summer of 2008.

Because we had only a relative small sample size of foliage biomass over the Porcupine caribou habitat, we didn't leave a fraction of the foliage biomass measurement points as validation. Nevertheless, we did find a similar relationship between Landsat-based simple ration and foliage biomass for the Bathurst caribou habitat located in Northwest Territory, Nunavut Territory, and northern Saskatchewan (Chen et al., 2011), with r^2 = 0.86, SEE = 26.3 g m^{-2}, F= 158, P = 2.6×10^{-12}, and n = 27.

3.5 Baseline maps of aboveground and foliage biomass

Applying equations (7) and (8) to the co-registered and geo-referenced Landsat and JERS-1/SAR mosaics data over the Porcupine caribou habitat, we produced aboveground biomass for the Porcupine caribou habitat. Fig. 9 shows aboveground biomass distribution in circa 2000 over the Porcupine caribou habitat.

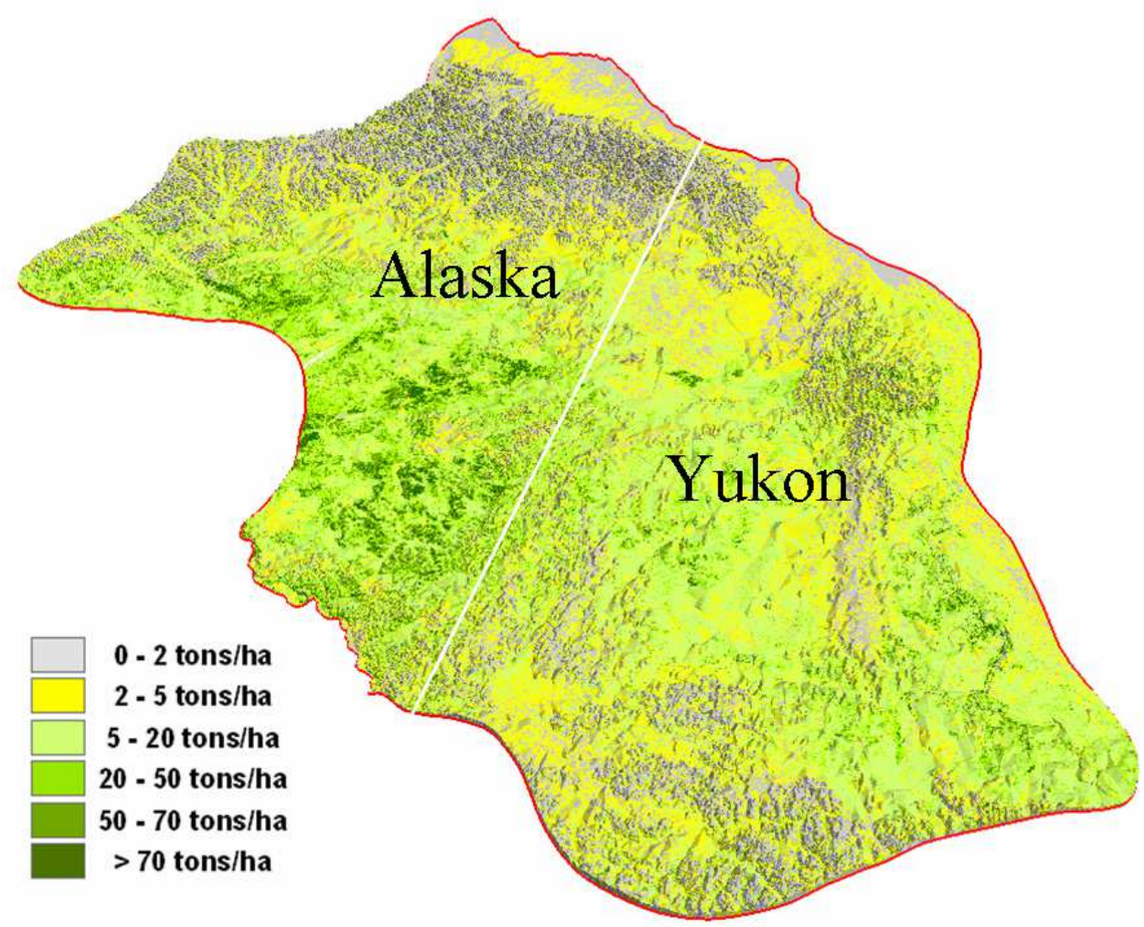

Fig. 9. Aboveground biomass distribution over the Porcupine caribou habitat circa 2000. The 3-d effect was generated using the DEM data.

The amount of aboveground biomass was less than 5 t ha^{-1} for most area of the Porcupine caribou calving ground located in northern coastal area in both Alaska and Yukon. Along the coastal line and at high mountain ridges, the aboveground biomass further decreased to less than 2 t ha^{-1}. For the summer and winter ranges of the Porcupine caribou habitat to the south, the values of aboveground biomass generally increased, with a large percentage of the areas having aboveground biomass in the range of 5-20 t ha^{-1}, as well as a significant fraction of the area of 2-5 t ha^{-1} aboveground biomass. The areas of aboveground biomass 2-5 t ha^{-1} appeared to be dominated by graminoids and herbs, while those of 5-20 t ha^{-1} aboveground biomass were mainly shrub land. The Porcupine summer and winter ranges also had a small fraction of area that had more than 20 t ha^{-1} aboveground biomass, likely associated with treed woodland. Areas of 0-2 t ha^{-1} aboveground biomass also occur in the summer and winter ranges of the Porcupine caribou habitat, mostly happened at high mountain ridges.

The information on foliage biomass can be more useful to local caribou management boards and researchers because it is directly related forage availability (Russell et al., 1993; Russell & McNeil, 2002; Russell et al., 2002). Using equation (9), we developed circa 2000 foliage biomass distribution over the Porcupine caribou habitat (Fig. 10).

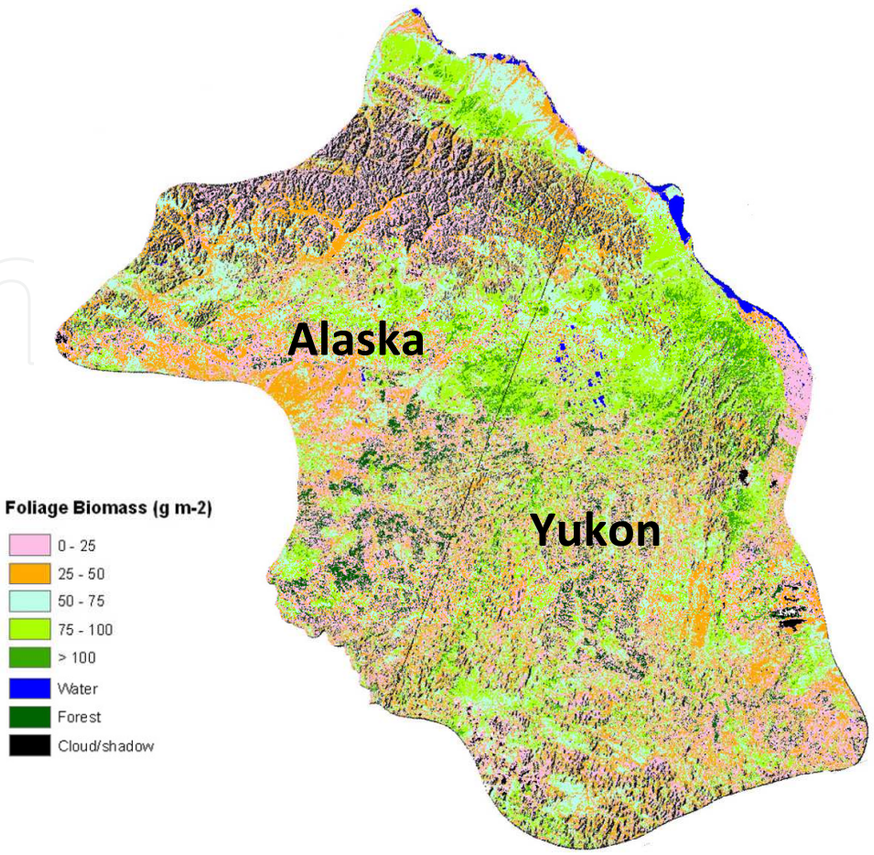

Fig. 10. Foliage biomass distribution over the Porcupine caribou habitat cirac 2000. The 3-d effect was generated using the DEM data. Areas covered by water, forest, and cloud were blocked out.

Fig. 10 shows the circa 2000 foliage biomass distribution of non-forest land areas in the Porcupine caribou habitat. Because of lacking foliage biomass measurements over forested land, foliage biomass was not estimated over forest areas in the Porcupine caribou habitat and areas covered forests were blocked out in Fig. 10. We also blocked out water and cloud-cover areas in Fig. 10. As shown in Fig. 10, most of the northern coastal areas in Alaska and Yukon, over which the calving ground of the Porcupine caribou habitat is located, had a quite high foliage biomass from 50 to > 100 g m^{-2}. This is a contrast to the distribution of the aboveground biomass. Over these same coastal areas the aboveground biomass was quite low. Both aboveground biomass and foliage biomass were found to be lower at high mountain ridges, and coastal beaches.

The foliage biomass map reveals that on average the amount of seasonal peak foliage biomass in the calving ground of the Porcupine caribou herd was similar to that in the summer range, and was even higher if only the concentrated calving ground over the Northern Alaska and Yukon coastal plain is concerned (Table 5). To the contrast, the average seasonal peak foliage biomass in the calving ground of the Bathurst caribou herd was much lower than that in the summer range during the same time period (Chen et al., 2011). This result agree well with the ground survey by Griffith et al. (2001), which suggested that on June 14, during 1998-1999, the total available forage was 63 g m^{-2} for the

Bathurst caribou calving ground, in comparison with 460 g m^{-2} for the Porcupine caribou calving ground. Of the 63 g m^{-2} forage over the Bathurst caribou calving ground, 33 g m^{-2} was lichen and moss, 14 g m^{-2} was stand dead, and only 16 g m^{-2} was vascular biomass. On the contrast for the Porcupine caribou calving ground, 50 g m^{-2} was lichen and moss, 250 g m^{-2} was stand dead, and 160 g m^{-2} was vascular biomass. The live biomass over the Porcupine calving ground was 10 time that over the Bathurst calving ground. In addition, the high value of stand dead over the Porcupine calving ground also suggest the high foliage biomass value over previous years. The difference in calving ground foliage biomass collaborates well with the fact that cows of the Bathurst herd leave calving ground soon after giving birth while those of Porcupine herd stay for a much longer period (Griffith et al., 2001).

	Porcupine	Bathurst	*Data sources*
Measured foliage biomass, calving ground (g m^{-2})	63 - 106	17 - 94	This study, Chen et al. (2011)
Area-averaged foliage biomass, calving ground (g m^{-2})	78	24	This study, Chen et al. (2011)
Measured foliage biomass, summer range (g m^{-2})	14 – 198	17 - 267	This study, Chen et al. (2011)
Area-averaged foliage biomass, summer range (g m^{-2})	69	43	This study, Chen et al. (2011)
Milk production (l d^{-1})	2.02	1.09 – 1.79	Griffith et al. (2001)
Calve growth rate (g d^{-2})	493	150 - 407	Griffith et al. (2001)
Cow body weight range (kg)	83 - 96	66 - 78	Griffith et al. (2001)

Table 5. Comparison of measured and area-averaged foliage biomass values between Porcupine caribou habitat and Bathurst caribou habitat. The area-averaged values were calculated from the circa 2000 baseline foliage biomass maps. Field measurement of foliage biomass over the Bathurst caribou habitat was conducted during the summer of 2005 (Chen et al., 2011). Also included in the comparison are cow milk production, calve growth rate, and cow body weight.

The difference in calving ground forage availability, in turn, results in difference in caribou biological measures (Table 5). For example, the body weights of Porcupine cows are about 20% higher than that of Bathurst herd (Griffith et al., 2001). The Bathurst cow milk production was 1.09 – 1.79 liter per day, against 2.02 liter per day by an average Porcupine caribou cow, with the corresponding calve growth rate being 150 -407 gram per day for the Bathurst herd against 493 gram per day for that of the Porcupine herd (Table 5).

4. Conclusions

Aboveground biomass was measured at 43 sites in the summer of 2004 along the Dempster Highway, which goes through the winter and summer ranges of the Porcupine caribou habitat. The measured aboveground biomass ranged 10-100 t ha^{-1} for sparsely forested woodlands, 1-100 t ha^{-1} for the low-high shrub sites, and 0.5-10 t ha^{-1} for mixed graminoids-dwarf shrub-herb sites.

Foliage biomass was measured at 10 non-forested sites along the Dempster Highway in the summer of 2006, and again in the summer of 2008 at 11 non-forested sites in the Ivvavik National Park located at northern tip of Yukon, which overlaps with the calving ground and summer range of the Porcupine caribou herd. The measured foliage biomass ranged 0.95-2 t ha^{-1} for low-high shrub sites, 0.38-0.92 t ha^{-1} for mixed graminoids-dwarf shrub-herb sites, 0.63-1.06 t ha^{-1} for coastal tussock sites, and < 0.2 t ha^{-1} for hill-top rock lichen sites.

When all data points were pooled together, the best relationship between aboveground biomass and remote sensing data was found to be with the combination of JERS-1 backscatter and Landsat B4/B5, with r^2 = 0.72. Validation using aboveground biomass measurements at foliage biomass measurement sites gives similar result, with the slope = 0.91, r^2 = 0.90, and *SEE* = 1.5 t h^{-1} over measured aboveground biomass range from 0 to 18.16 t h^{-1}. Similar validation results were obtained using aboveground biomass measurements at 33 sites around Yellowknife, Northwest Territories, and Lupin Gold Mine, Nunavut Territories in a previous study (Chen et al., 2009a), with r^2 = 0.81, slope =1.17, and *SEE* = 9.67 t h^{-1} over measured aboveground biomass range from 0.9 to 103.3 t h^{-1}.

For the foliage biomass, the Landsat-based simple ration gives the best fit, with r^2 = 0.81, *SEE* = 20.6 g m^{-2}, *F*= 81, $P = 2.7\times10^{-8}$, and *n* = 21.

Appling these relationships to the mosaic of Landsat and JERS-1 images covering the entire Porcupine caribou habitat, we produced baseline maps of aboveground biomass and foliage biomass for the Porcupine caribou habitat. The foliage biomass map reveals that on average the amount of seasonal peak foliage biomass in the calving ground of the Porcupine caribou herd was similar to that in the summer range, and was even higher if only the concentrated calving ground over the Northern Alaska and Yukon coastal plain is concerned. To the contrast, the average seasonal peak foliage biomass in the calving ground of the Bathurst caribou herd was much lower than that in the summer range during the same time period. The difference in calving ground foliage biomass collaborates well with the fact that cows of the Bathurst herd leave calving ground soon after giving birth while those of Porcupine herd stay for a much longer period, which in turn partially explain why the Porcupine caribou calves can have several times higher growth rate and the body weights of Porcupine cows are about 20% higher than that of Bathurst herd.

It should be emphasized, however, that assessment of the impacts of climate change on the Porcupine caribou habitat requires integration of various information sources from remote sensing products, climate records, and other relevant tempo-spatial data. Furthermore, there are many other factors besides the habitat, such as harvest, predators, diseases/parasites, industrial development, extreme weather events, climate change, and pollution, may influence the abundance of a caribou herd. Therefore, this work is just one of the first steps towards informed and proper decision-making that balances the needs of caribou habitat protection and industrial development under a global change environment.

5. Acknowledgment

This study is financially supported by grants from the Canadian IPY program through a project entitled "Climate Change Impacts on Canadian Arctic Tundra Ecosystems (CiCAT): Interdisciplinary and Multi-scale Assessments", Canadian Space Agency's Government Related Initiatives Program (GRIP) through a project entitled "ParkSPACE: Towards an Operational Satellite-based System for Monitoring Ecological Integrity of Arctic National Parks", and from the Earth Sciences Sector, NRCan's "Climate Change Geosciences

Program". Colleagues from CARMA (e.g., Drs. Don Russell, Wendy Nixon, and Brad Griffith) have provided great insights about research priorities and directions on caribou habitats. Parks Canada Agency (e.g., Dr. Don McLennan, Paul Dixon, et al.) organized 2008 field work in the Ivvavik National Park, arranged licence application, and provided logistics supports including helicopter riding and camping facility. David Jones and 3 northern students from Aklavik, NWT (Alexander Gordon, Jayneta Pascal, Kayla Arey) participated in and contributed his through knowledge of northern vegetation to the field measurement campaign in the summers of 2004, 2006, or 2008. Drs. Kyle McDonald of the Jet Propel Laboratory/NASA and Mahta Moghaddam of University of Michigan provided the JERS coverage over Canada's north. The Aurora Research institute and the Gwich'in Renewable Resource Board, Inuvik, NWT helped us in obtaining research licenses. Steve Wolfe of the Geological Survey Canada arranged the use of the laboratory space and biomass drying ovens. Drs. Yinsuo Zhang and Nadia Rochdi provided critical reviewed of the manuscript. The authors wish to thank all for providing their assistances.

6. References

Anderson, G.L. & Hanson, J.D. (1992). Evaluating handheld radiometer derived vegetation indices for estimating above ground biomass. *Geocarto International*, Vol. 7, pp. 71–78.

Anderson, G.L.; Hanson, J.D. & Haas, R.H. (1993) Evaluating Landsat Thematic Mapper derived vegetation indices for estimating aboveground biomass on semiarid rangelands. *Remote Sensing of Environment*, Vol. 45, pp. 165–175.

Balzter, H. (2001) Forest mapping and monitoring with interferometric synthetic aperture radar (InSAR). *Progress in Physical Geography*, Vol. 25, pp. 159–177.

Brown, L.; Chen, J.M.; Leblanc, S.G. & Cihlar, J. (2000). A shortwave infrared modification to the simple ratio for LAI retrieval in boreal forests: an image and model analysis. *Remote Sensing of Environment*, Vol. 71, pp. 16–25.

Castel, T.; Guerra, F.; Caraglio, Y. & Houllier, F. (2002) Retrieval biomass of a large Venezuelan pine plantation using JERS-1 SAR data: analysis of forest structure impact on radar signature. *Remote Sensing of Environment*, Vol. 79, pp. 30–41.

Chen, J.M. & Cihlar, J. (1996). Retrieving leaf area index of boreal conifer forests using Landsat TM images. *Remote Sensing of Environment*, Vol. 55, pp. 153–162.

Chen, J.M.; Pavlic, G., Brown, L.; Cihlar, J.; Leblanc, S.G.; White, H.P.; Hall, R.J.; Peddle, D.R.; King, D.J.; Trofymow, J.A.; Swift, E.; Van der sanden, J. & Pellikka, P.K.E. (2002). Derivation and validation of Canada-wide coarse resolution leaf area index maps using high-resolution satellite imagery and ground measurements. *Remote Sensing of Environment*, Vol. 80, pp. 165–184.

Chen, W. (2004). Tree size distribution functions of four boreal forest types for biomass mapping. *Forest Science*, Vol. 50, pp. 436-449.

Chen, W.; Blain, D.; Li, J.; Keohler, K.; Fraser, R.; Zhang, Y.; Leblanc, S.G.; Olthof, I.; Wang, J. & McGovern, M. (2009a). Biomass measurements and relationships with Landsat-7/ETM+ and JERS-1/SAR data over Canada's western sub-arctic and low arctic. *International Journal of Remote Sensing*, Vol. 30, No. 9, pp. 2355—2376.

Chen, W.; Li, J.; Zhang, Y.; Zhou, F.; Koehler, K.; Leblanc, S.; Fraser, R.; Olthof, I.; Zhang, Y. & Wang, J. (2009b). Relating biomass and leaf area index to non-destructive

measurements for monitoring changes in arctic vegetation. *Arctic*, Vol. 62, No. 3, pp. 281–294

Chen, W.; Russell, D.E.; Gunn, A.; Croft, B.; Li, J.; Chen, W.R.; Zhang, Y.; Koehler, K.; Olthof, I.; Fraser, R.H.; Leblanc, S.G.; Henry, G.R.; White, R.G. & Finstad, G.L. (2011). Migratory tundra caribou habitat quality indicators and relationships with climate: calving ground and summer range. *Climatic change* (submitted).

Chen, W.R.; Chen W. & Li, J. (2010a). Comparison of surface reflectance derived by relative radiometric normalization versus atmospheric correction for generating large-scale Landsat mosaics. *Remote Sensing Letters*, Vol. 1, No. 2, pp. 103 – 109.

Chen, Z.; Chen, W.; Leblanc, S.G. & Henry, G. (2010b). Digital photograph analysis for measuring percent plant cover in the Arctic. *Arctic* Vol. 63, No. 3, pp. 315-326.

Evert, F. (1985). *Systems of equations for estimating oven-dry mass of 18 Canadian tree species*. Canadian Forestry Service, Petawawa National Forestry Institute.

Foody, G.M.; Boyd, D.S. & Culter, M.E.J. (2003). Predictive relations of tropical forest biomass from Landsat TM data and their transferability between regions. *Remote Sensing of Environment*, Vol. 85, pp. 463 – 474.

Franklin, J. & Hiernaux, P.Y.H. (1991). Estimating foliage and woody biomass in Sahelian and Sudanian woodlands using a remote sensing model. *International Journal of Remote Sensing*, Vol. 12, pp. 1387–1404.

Gould, W.A.; Raynolds, M. & Walker, D.A. (2003). Vegetation, plant biomass, and net primary productivity patterns in the Canadian Arctic. *Journal of Geophysical Research*, 108(D2), 8167, doi:10.1029/2001JD000948.

Griffith, B.; Douglas, D.; Walsh, N.; Young, D.; McCabe, T.; Russell, D.E.; White, R.G.; Cameron, R. & Whitten K (2002). The Porcupine caribou herd. In: *Arctic Refuge coastal plain terrestrial wildlife research summaries*. D. Douglas; P. Reynolds & E. Rhode (Eds.). U.S. Geological Survey, Biological Science Report BSR-2002-0001.

Griffith, B.; Gunn, A.; Russell, D.E.; Johnstone. J.; Kielland, K.; Wolfe, S. & Douglas, D.C. (2001). *Bathurst caribou calving ground studies: Influence of nutrition and human activity on calving ground location*. Final report submitted to West Kitikmeot Slave Study Society, Yellowknife, NWT, Canada, pp 90.

Hall, E. (Ed.) (1989) *People & Caribou in the Northwest Territories*. Government of Northwest Territories, Department of Renewable Resources, Yellowknife, NWT, Canada.

Hall, F.G.; Shimabukura, Y.E. & Huemmrich, K.F. (1995). Remote sensing of forest biophysical structure using mixture decomposition and geometric reflectance models. *Ecological Applications*, Vol. 5, pp. 993–1013.

Halliwell, D.H. & Apps, M.J. (1997). *BOREAS biometry and auxiliary sites: over story and under story data*. Natural Resources Canada, Canadian Forest Service, Northern Forest Centre, Edmonton, Alberta, Canada, pp. 244.

Heiskanen, J. (2006). Estimating aboveground tree biomass and leaf area index in a mountain birch forest using ASTER satellite data. *International Journal of Remote Sensing*, Vol. 27, No. 6, pp. 1135–1158.

Heuer, K. (2006). *Being Caribou: Five Months on Foot with an Arctic Herd*. McClelland & Stewart Ltd., Toronto, ON, Canada, pp. 235.

Kaiser, J. (2002). Caribou study fuels debate on drilling in Arctic Refuge. *Science*, Vol. 296, pp. 444-445.

Kasischke, E.S.; Goetz, S.; Hansen, M.C.; Ustin, S.L.; Ozdogan, M.; Woodcock, C.E. & Rogan, J. (2004). Temperate and boreal forests. In: *Remote Sensing for Natural Resource Management and Environmental Monitoring*, S.L. Ustin (Ed.), pp. 147–238, John Wiley & Sons Hoboken, New Jose, USA.

Kuplich, T.M.; Salvatori, V. & Curran, P.J. (2000). JERS-1/SAR backscatter and its relationship with biomass of regenerating forests. *International Journal of Remote Sensing*, Vol. 21, pp. 2513 – 2518.

Kurvonen, L.; Pulliainen, J. & Hallikainen, M. (1999). Retrieval of biomass in boreal forests from multitemporal ERS-1 and JERS-1 SAR data. *IEEE Transactions on Geoscience and Remote Sensing*, Vol. 37, pp. 198–205.

Laidler, G.J. & Treitz, P. (2003). Biophysical remote sensing of arctic environments. *Progress in Physical Geography*, Vol. 27, pp. 44-68.

Le Toan, L.; Beaudoin, A.; Riom, J. & Guyon, D. (1992). Relating forest biomass to SAR data. *IEEE Transactions on Geoscience and Remote Sensing*, Vol. 30, pp. 403 – 411.

Lee, N.J. & Nakane, K. (1996). Forest vegetation classification and biomass estimation based on Landsat-TM data in a mountainous region of west Japan. In: *The Use of Remote Sensing in The Modeling of Forest Productivity*, H.L. Gholz, K. Nakane & H. Shimoda (Eds.), pp. 159 – 171, Kluwer Academic Publishers, Dordrecht, The Netherlands.

Linder, W. & Meuser, H.F. (1993). Automatic tiepointing in SAR images. In: *SAR Geocoding: Data and Systems*, G. Schreier (Ed.), pp. 202 – 212, Karlsruhe, Wichmann, Germany.

Lu, D. (2005). Aboveground biomass estimation using Landsat TM data in the Brazilian Amazon Basin. *International Journal of Remote Sensing*, Vol. 26, pp. 2509–2525.

Lu, D.; Mausel, P.; Brondizio, E. & Moran, E. (2004) Relationships between forest stand parameters and Landsat Thematic Mapper spectral responses in the Brazilian Amazon basin. *Forest Ecology and Management*, Vol. 198, pp. 149–167.

Luckman, A.; Baker, J.R.; Kuplich, T.M.; Yanasse, C.C.F. & Frery, A.C. (1997). A study of the relationship between radar backscatter and regenerating forest biomass for space borne SAR instrument. *Remote Sensing of Environment*, Vol. 60, pp. 1–13.

Lucus, R.M.; Held, A.A.; Phinn, S.R. & Saatchi, S. (2004). Tropical forests. In: *Remote Sensing for Natural Resource Management and Environmental Monitoring*, S.L. Ustin (Ed.), pp. 239–315, John Wiley & Sons, Hoboken, New Jose, USA.

Madsen, K. (2001). *Project Caribou: An Educator's Guide to Wild Caribou of North America.* Department of Renewable Resources, Government of Yukon, Whitehorse, Yukou Territories, Canada.

Moghaddam, M.; Dungan, J.L. & Acker, S. (2002). Forest variable estimation from fusion of SAR and multispectral optical data. *IEEE Transactions on Geoscience and Remote Sensing*, Vol. 40, pp. 2176 – 2187.

Mutanga, O. & Skidmore, A.K. (2004). Narrow band vegetation indices overcome the saturation problem in biomass estimation. *International Journal of Remote Sensing*, Vol. 25, pp. 3999–4014.

National Research Council, (2003). *Cumulative Environmental Effects of Oil and Gas Activities on Alaska's North Slope*. The National Academies Press, Washington DC, USA.

Nelson, R.F.; Kimes, D.S.; Salas, W.A. & Routhier, M. (2000). Secondary forest age and tropical forest biomass estimation using Thematic Mapper imagery. *Bioscience*, Vol. 50, pp. 419–431.

Olthof, I.; Pouliot, D.; Fernandes, R. & Latifovic, R. (2005). Landsat-7 ETM+ radiometric normalization comparison for northern mapping applications. *Remote Sensing of Environment*, Vol. 95, pp. 388-398.

Phua, M. & Saito, H. (2003). Estimation of biomass of a mountainous tropical forest using Landsat TM data. *Canadian Journal of Remote Sensing*, Vol. 29, pp. 429 – 440.

Ranson, K.; Sun, G.; Lang, R.H.; Chauhan, N.S.; Cacciola, R.J. & Kilic, O. (1997). Mapping of boreal forest biomass from spaceborne synthetic aperture radar. *Journal of Geophysical Research*, Vol. 102, pp. 29599 – 29610.

Rauste, Y.; Hame, T.; Pulliainen, J.; Heiska, K. & Hallikainen, M. (1994). Radar-based forest biomass estimation. *International Journal of Remote Sensing*, Vol. 15, pp. 2797 – 2808.

Russell, D.E. & McNeil, P. (2002). *Summer ecology of the Porcupine caribou herd*. Porcupine Caribou Management Board, Whitehorse, Yukon Territories, Canada

Russell, D.E.; Kofinas, G. & Griffith, B. (2002). *Barren-Ground Caribou Calving Ground Workshop: Report of Proceedings*. Technical Report Series No. 390, Canadian Wildlife Service, Ottawa, Ontario, Canada.

Russell, D.E.; Martell, A.M. & Nixon, W.A.C. (1993). Range ecology of the Porcupine caribou herd in Canada. *Rangifer*, special issue No. 8.

Russell, D.E.; Whitten, K.R.; Farnell, R. & van de Wetering, D. (1992). *Movement and distribution of the Porcupine caribou herd, 1970-1990*. Technical Report Series No 138, Environment Canada, Canadian Wildlife Service, Whitehorse, Yukon Territoies, Canada.

Sader, S.A. (1987). Forest biomass, canopy structure, and species composition relationships with multipolarization L-band synthetic aperture radar data. *Photogrammetric Engineering and Remote Sensing*, Vol. 53, pp. 193–202.

Sader, S.A.; Waide, R.B.; Lawrence, W.T. & Joyce, A.T. (1989). Tropical forest biomass and successional age class relationships to a vegetation index derived from Landsat-TM data. *Remote Sensing of Environment*, Vol. 28, pp. 143–156.

Santos, J.R.; Pardi Lacruz, M.S.; Araujo, L.S. & Keil, M. (2002). Savanna and tropical rainforest biomass estimation and spatialization using JERS-1 data. *International Journal of Remote Sensing*, Vol. 23, pp. 1217–1229.

Serreze, M.C.; Walsh, J.E.; Chapin III, F.S.; Osterkamp, T.; Dyurgerov, M.; Romanovsky, V.; Oechel, W.C.; Morison, J.; Zhang, T. & Barry, R.G. (2000). Observational evidence of recent change in the northern high-latitude environment. *Climatic Change*, Vol. 46, pp. 159-207.

Sheng, Y. & Alsdorf, D.E. (2005). Automated georeferencing and orthorectification of Amazon basin-wide SAR mosaics using SRTM DEM data. *IEEE Transactions on Geoscience and Remote Sensing*, Vol. 43, pp. 1929 – 1940.

Sprugel, D.G. (1983). Correcting for bias in log-transformed allometric equations. *Ecology*, Vol. 64, pp. 209-210.

Steininger, M.K. (2000). Satellite estimation of tropical secondary forest aboveground biomass data from Brazil and Bolivia. *International Journal of Remote Sensing*, Vol. 21, pp. 1139–1157.

Sturm, M.; Racine, C. & Tape, K. (2001). Increasing shrub abundance in the Arctic. *Nature*, Vol. 411, pp. 546– 547.

Sun, G.; Ranson, K.J. & Kharuk, V.I. (2002). Radiometric slope correction for forest biomass estimation from SAR data in the western Sayani Mountains, Siberia. *Remote Sensing of Environment*, Vol. 79, pp. 279–287.

Theau, J.; Peddle, D.R. & Duguay, C.R. (2005). Mapping lichen in a caribou habitat of Northern Quebec, Canada, using an enhancement-classification method and spectral mixture analysis. *Remote Sensing of Environment*, Vol. 94, pp. 232–243.

Tsolmon, R.; Tateishi, R., & Tetuko, J.S.S. (2002). A method to estimate forest biomass and its application to monitor Mongplian Taiga using JERS-1 SAR data. *International Journal of Remote Sensing*, Vol. 23, pp. 4971 – 4978.

Turner, D.P.; Cohen, W.B.; Kennedy, R.E.; Fassnacht, K.S. & Briggs, J.M. (1999). Relationships between leaf area index and Landsat TM spectral vegetation indices across three temperate zone sites. *Remote Sensing of Environment*, Vol. 70, pp. 52–68.

Walker, D.A.; Epstein, H.E.; Jia, G.J.; Balser, A.; Copass, C.; Edwards, E.L.; Gould, W.A.; Hollingsworth, J.; Knudson, J.; Maier, H.A.; Moody, A. & Raynolds, M.K. (2003). Phytomass, LAI, and NDVI in northern Alaska: Relationships to summer warmth, soil pH, plant functional types and extrapolation to the circumpolar Arctic. *Journal of Geophysical Research*, 108 (D2), 8169, doi: 10.1029/ 2001JD000986.

Wylie, B.K.; Meyer, D.J.; Tieszer, L.L. & Mannel, S. (2002). Satellite mapping of surface biophysical parameters at the biome scale over the North American grasslands, a case study. *Remote Sensing of Environment*, Vol. 79, pp. 266–278.

Zheng, D.; Rademacher, J.; Chen, J.; Crow, T.; Bresee, M.; Moine, J.L. & Ryu, S.R. (2004). Estimating aboveground biomass using Landsat 7 ETM+data across a managed landscape in northern Wisconsin, USA. *Remote Sensing of Environment*, Vol. 93, pp. 402 – 411.

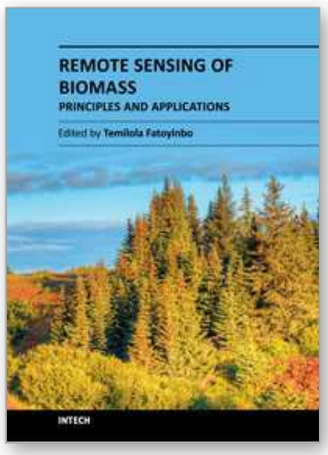

Remote Sensing of Biomass - Principles and Applications
Edited by Dr. Lola Fatoyinbo

ISBN 978-953-51-0313-4
Hard cover, 322 pages
Publisher InTech
Published online 28, March, 2012
Published in print edition March, 2012

The accurate measurement of ecosystem biomass is of great importance in scientific, resource management and energy sectors. In particular, biomass is a direct measurement of carbon storage within an ecosystem and of great importance for carbon cycle science and carbon emission mitigation. Remote Sensing is the most accurate tool for global biomass measurements because of the ability to measure large areas. Current biomass estimates are derived primarily from ground-based samples, as compiled and reported in inventories and ecosystem samples. By using remote sensing technologies, we are able to scale up the sample values and supply wall to wall mapping of biomass. Three separate remote sensing technologies are available today to measure ecosystem biomass: passive optical, radar, and lidar. There are many measurement methodologies that range from the application driven to the most technologically cutting-edge. The goal of this book is to address the newest developments in biomass measurements, sensor development, field measurements and modeling. The chapters in this book are separated into five main sections.

INTECH
open science | open minds

InTech Europe
University Campus STeP Ri
Slavka Krautzeka 83/A
51000 Rijeka, Croatia
Phone: +385 (51) 770 447
Fax: +385 (51) 686 166
www.intechopen.com

InTech China
Unit 405, Office Block, Hotel Equatorial Shanghai
No.65, Yan An Road (West), Shanghai, 200040, China
中国上海市延安西路65号上海国际贵都大饭店办公楼405单元
Phone: +86-21-62489820
Fax: +86-21-62489821

IntechOpen